# Spatiotemporal Dynamics and Reliable Computations in Recurrent Spiking Neural Networks

Ryan Pyle[1] and Robert Rosenbaum[1,2]
[1]Department of Applied and Computational Mathematics and Statistics, University of Notre Dame, Notre Dame, Indiana 46556, USA
[2]Interdisciplinary Center for Network Science and Applications, University of Notre Dame, Notre Dame, Indiana 46556, USA
(Received 26 August 2016; revised manuscript received 4 November 2016; published 6 January 2017)

Randomly connected networks of excitatory and inhibitory spiking neurons provide a parsimonious model of neural variability, but are notoriously unreliable for performing computations. We show that this difficulty is overcome by incorporating the well-documented dependence of connection probability on distance. Spatially extended spiking networks exhibit symmetry-breaking bifurcations and generate spatiotemporal patterns that can be trained to perform dynamical computations under a reservoir computing framework.

DOI: 10.1103/PhysRevLett.118.018103

Biological neuronal networks exhibit irregular and asynchronous activity [1,2] that is often modeled using randomly connected networks of excitatory and inhibitory spiking neurons. In these models, an approximate balance between excitation and inhibition combines with random connectivity to produce asynchronous-irregular spiking activity similar to that observed in experimental recordings [3–6].

Despite their ability to explain the genesis of neural variability, asynchronous-irregular spiking network models have a critical shortcoming: Their microscopic dynamics—at the level of spike times—are intricate and nonlinear, but largely unreliable [3,4,7,8]. Their macroscopic dynamics—at the level of firing rates—are reliable, but primarily track network input [3,4,6,9,10]. Biological neural networks must generate reliable, intricate responses to simple sensory inputs, for example, to produce motor output [11,12]. This raises the question of how neural circuits reliably produce intricate firing rate dynamics for dynamical computations.

In this Letter, we show that the limited dynamical complexity of firing rates in asynchronous-irregular spiking networks is overcome by incorporating the widely reported dependence of connection probability on distance [13–16]. Spiking networks with a spatial topology can undergo symmetry-breaking Turing-Hopf bifurcations [17,18] to generate intricate spatiotemporal dynamics that can be trained to perform computations.

*Results*.—Following previous work [9], we consider a recurrent neural network with $4\times10^4$ excitatory ($e$) and $10^4$ inhibitory ($i$) model neurons arranged uniformly on a square-shaped domain, $\Gamma=[0,1]\times[0,1]$, with periodic boundaries, i.e., a torus. The synaptic input current to neuron $j$ in population $a=e,i$ is given by

$$I_j^a(t)=\sum_{k=1}^{N_e}J_{jk}^{ae}\sum_n\delta(t-t_{nk}^e)+\sum_{k=1}^{N_i}J_{jk}^{ai}\sum_n\delta(t-t_{nk}^i)+F_j^a(t),$$

where $t_{nk}^b$ is the $n$th spike of neuron $k$ in population $b=e,i$. Spikes are determined by a leaky integrate-and-fire dynamic [19]. To model the widely observed distance dependence of connection probability [13–16], the synaptic weight from a neuron at coordinates $\mathbf{y}\in\Gamma$ in population $b$ to a neuron at $\mathbf{x}\in\Gamma$ in population $a$ is chosen randomly according to

$$J_{jk}^{ab}=\begin{cases}j_{ab} & \text{with prob. } p_{ab}(\mathbf{x}-\mathbf{y})\\ 0 & \text{otherwise}\end{cases},$$

where $p_{ab}(\mathbf{u})=\bar{p}_{ab}G(\mathbf{u};\sigma_b)$ and $G(\mathbf{u};\sigma_b)$ is a two-dimensional wrapped Gaussian with width $\sigma_b$ [9].

We first simulated a network in which external inputs were constant across space and time and inhibitory projections were more localized than excitatory projections [Fig. 1(a)]. Even though the model is deterministic, spiking activity was irregular and asynchronous with no coherent spatial patterning [Fig. 1(b), Supplemental Material at Figs. 1 and 2 and Supplemental animation]. This spike-timing variability is driven by chaoslike dynamics [3,4,7–9].

Despite the complexity of spike-timing dynamics, firing rates are amenable to mean-field analysis under a diffusion approximation [9]. The mean input, $\vec{\mu}(\mathbf{x})=[\mu_e(\mathbf{x})\ \mu_i(\mathbf{x})]^T$, to $e$ and $i$ neurons near $\mathbf{x}\in\Gamma$ is

$$\vec{\mu}(\mathbf{x})=\iint_\Gamma W(\mathbf{u})\vec{r}(\mathbf{x}-\mathbf{u})d\mathbf{u}+\vec{F}(\mathbf{x}),$$

where $\vec{r}(\mathbf{x})=[r_e(\mathbf{x})\ r_i(\mathbf{x})]^T$ is the average firing rate and $\vec{F}(\mathbf{x})$ the feedforward input to neurons near $\mathbf{x}\in\Gamma$. The matrix kernel $W(\mathbf{u})$ captures synaptic divergence and similarly for the input variance, $v(\mathbf{x})=\iint U(\mathbf{u})\vec{r}(\mathbf{x}-\mathbf{u})d\mathbf{u}$ [20]. The mapping from input statistics to rates, $\vec{r}=\phi(\vec{\mu},\vec{v})$, is computed using a Fokker-Planck formalism so fixed point rates can be computed numerically [21–24]. When $\vec{F}(\mathbf{x})=\vec{F}$ is spatially uniform, so are fixed point rates [9].

To estimate local rates from simulations, we partitioned the network into 100 squares, then averaged and low-pass

 © 2017 American Physical Society

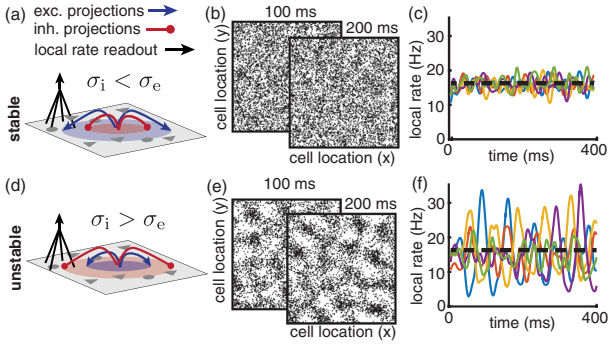


FIG. 1. Intrinsic dynamics in a spatially extended spiking network. (a) Schematic of spatially extended spiking network model. Excitatory and inhibitory neurons arranged on a square project randomly to one another. Lateral excitatory projections (blue) are longer on average than lateral inhibitory projections (red; $\sigma_e = 0.1$, $\sigma_i = 0.05$, $F^e(t) = 3$ V/s, $F^i(t) = 2.3$ V/s). Each local rate readout (black) is computed by averaging the activity of all excitatory neurons within a square patch then low-pass filtering with a Gaussian kernel ($\sigma = 5$ ms). (b) Raster plot snapshots over 5 ms time windows starting at $t = 100$ and 200 ms. (c) Five randomly chosen local rate readouts. Dashed black line shows numerically computed fixed point rate. (d)–(f) Same as (a)–(c), but inhibitory projections are broader than excitatory ($\sigma_e = 0.05$, $\sigma_i = 0.1$). See Supplemental animation for animated raster plots.

filtered the spike trains of the 400 excitatory neurons in each square [Fig. 1(a)]. These local rate readouts closely matched the fixed point rates computed numerically from the diffusion approximation [Fig. 1(c)] and fluctuations in the rates were consistent with asynchronous, Poisson-like spike timing variability [25].

Broad lateral inhibition is known to induce spatial pattern formation [9,26–30]. We next modified the network so that inhibitory projections were broader than excitatory projections [Fig. 1(d)]. This produced a dramatic change in the spiking activity, with spatially uniform activity giving way to intricate, asymmetric spatiotemporal activity patterns [Fig. 1(e) and Supplemental animation], despite the spatial symmetry of connection probabilities in the network. These spatiotemporal patterns were reflected in the local rate readouts by irregular high-amplitude fluctuations [Fig. 1(f)]. Despite their differences, both networks produced asynchronous, irregular spike trains with an approximate balance between excitation and inhibition [31], though previous work suggests that the network would not maintain balance as network size diverges [9].

The network with broad inhibition and the network with local inhibition share the same spatially uniform fixed point under the diffusion approximation, but rates strongly deviated from this fixed point when inhibition was broader. We conjectured that the fixed point was stable for the simulation with local inhibition and unstable when inhibition was broader.

Spatially extended neural networks are often described using integrodifferential equations of the form

$$\tau_r \partial \vec{r}/\partial t = -\vec{r} + \phi(\vec{\mu}, \vec{v}), \tag{1}$$

or of a similar form. As in previous work [9], this approach predicted stability of uniform firing rates for the network with broad inhibition, despite the patterns observed in simulations [32]. We conjectured that firing rate dynamics observed when inhibition was broad arose in part from a resonance in neurons' membrane and spiking dynamics [33] that is not captured by Eq. (1). To account for this resonance, we generalized the stability analysis from recent work [34] to spatial networks. Linear response theory gives an integral equation for the dynamics of a perturbation from the fixed point [35],

$$\delta\vec{r}(\mathbf{x},t) = \iint_\Gamma \int_0^\infty A(\tau)W(\mathbf{u})\delta\vec{r}(\mathbf{x}-\mathbf{u},t-\tau)d\tau d\mathbf{u} + \iint_\Gamma \int_0^\infty B(\tau)U(\mathbf{u})\delta\vec{r}(\mathbf{x}-\mathbf{u},t-\tau)d\tau d\mathbf{u} \tag{2}$$

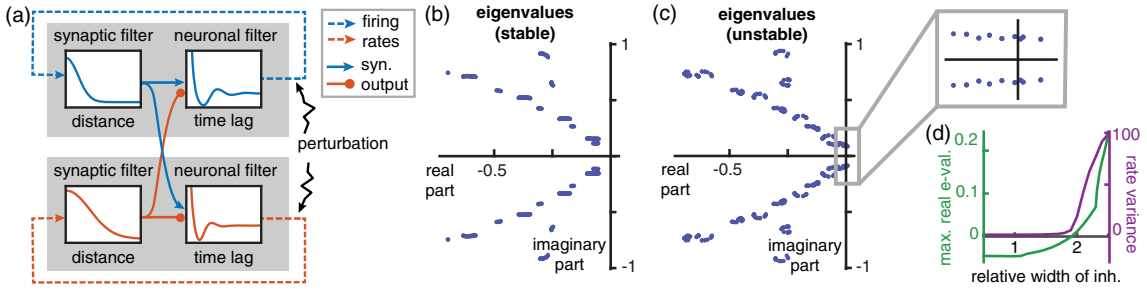


FIG. 2. Stability of spatially extended spiking networks. (a) Schematic of stability analysis. A perturbation applied to the firing rates (dashed lines, blue for excitatory and red for inhibitory) is filtered spatially by synaptic divergence (left boxes, showing connection probability as a function of distance) to determine perturbations of synaptic currents (solid lines), which are filtered temporally by neurons (right boxes, showing linear response kernels). (b) When inhibition is more local than excitation [as in Figs. 1(a)–1(c)], all eigenvalues have negative real parts. (c) Same as (b), except for broad inhibition [as in Fig. 1(d)–1(f)]. Some eigenvalues have positive real part (inset). (d) Maximum real part of the eigenvalues (green) and the average temporal variance of the firing rate readouts (purple; units $Hz^2$) as a function of the relative width of inhibitory projections ($\sigma_i/\sigma_e$).

as schematicized in Fig. 2(a). The matrix kernels, $A(\tau)$ and $B(\tau)$, quantify excitatory and inhibitory neurons' linear response to perturbations in their input mean and variance [36]. Equation (2) can capture an arbitrary linear dependence of firing rates on their history, which is generally not possible in a finite system of integrodifferential equations like Eq. (1). Transitioning to the temporal Laplace and spatial Fourier domains in Eq. (2) gives the Evans function [37]

$$\det[\hat{A}(\lambda)\tilde{W}(\mathbf{n}) + \hat{B}(\lambda)\tilde{U}(\mathbf{n}) - Id] = 0, \tag{3}$$

where $Id$ is the $2 \times 2$ identity matrix, $\tilde{W}(\mathbf{n})$ and $\tilde{U}(\mathbf{n})$ are Fourier coefficients of $W(\mathbf{u})$ and $U(\mathbf{u})$, and $\hat{A}(\lambda)$ and $\hat{B}(\lambda)$ are matrices of susceptibility functions [38], which can be computed under the diffusion approximation using a Fokker-Planck formalism [22–24,39]. Solutions, $\lambda$, to Eq. (3) are eigenvalues of the rate dynamics and the associated Fourier modes, $\mathbf{n}$, are eigenmodes.

Numerical computation of the eigenvalues confirms that the uniform fixed point rates are stable for the network with local inhibition [Fig. 2(b)] and unstable for the network with broad inhibition [Fig. 2(c)]. The eigenvalues with positive real part are complex [Fig. 2(c)] and are associated with nonuniform eigenmodes ($\mathbf{n} \neq 0$), implying a Turing-Hopf bifurcation that produces spatially coherent, time-varying patterns [17,18]. Varying the width of inhibition shows that eigenvalues with positive real part emerge once inhibition is about twice as broad as excitation, coinciding with the emergence of high-amplitude firing rate variability in simulations [Fig. 2(d), compare green and purple]. Stability can also be modulated by the strength of external input to inhibitory neurons [40], showing that the network's dynamical state can be controlled by input.

So far, we have considered purely spontaneous rate dynamics. We next added a time-varying external input shared by all neurons [Fig. 3(a)]. For the stable network, local rates approximately tracked the shared input with the addition of irregular fluctuations [Fig. 3(b)], consistent with Poisson-like spike-timing variability [41]. Applying principal component (PC) analysis to the local rates revealed that the majority of firing rate variability is captured by the first PC projection [Fig. 3(c)], representing the variability inherited from the one-dimensional external input. The remaining variability was spread among higher PC projections, representing spatially unstructured variability.

The unstable network exhibited a starkly different response to the external input. While local rates were affected by the external input, they did not reliably track it [Fig. 3(d)]. The input evoked a high-dimensional response, with variability distributed across several PC projections [Fig. 3(e)]. These results show that the unstable network generates high-dimensional firing rate dynamics in response to a one-dimensional input, while the stable network simply tracks the input with Poisson-like spike timing variability.

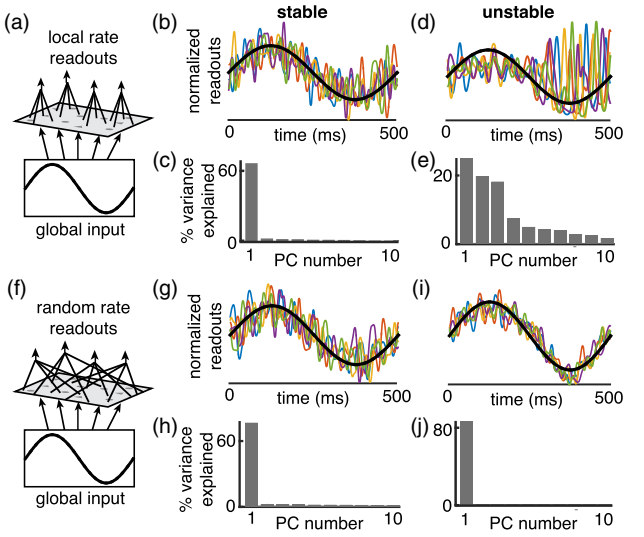


FIG. 3. Firing rate response to global input. (a) A spatially uniform sinusoidal input was provided to all neurons in the network [$F^e(t) = 3 + 1.5\sin(2\pi t)$, $F^i(t) = 2.3 + 1.5\sin(2\pi t)$]. (b) Five randomly chosen firing rate readouts (colored curves) track the input (black curve) with Poisson-like variability. All curves normalized by subtracting their mean and dividing by the standard deviation. (c) Percent variance in the 100 firing rate readouts explained by the first ten principal component projections. (d),(e) Same as (b) and (c), but for the unstable network. (f)–(j) Same as (a)–(e) except that firing rates are read out randomly and globally from the network.

While *local* rate readouts of the unstable network did not track the input, random *global* readouts from the same network do track input. We computed firing rate readouts generated from 400 excitatory neurons selected randomly from the entire network [Fig. 3(f)], instead of locally. These random readouts from both the stable and unstable networks reliably tracked external input [Figs. 3(g)–3(j)]. This finding can be understood by noting that the random readouts estimate the network-averaged rates. Equation (3) is identical for the stable and unstable networks at the uniform eigenmode, $\mathbf{n} = \mathbf{0}$, so the networks have the same eigenvalues at that mode. Hence, the global average firing rate exhibits similar dynamics in both networks.

For the rate dynamics generated by the unstable network to perform reliable computations, the response of the network should be consistent across repeated presentations of the same input. We found that the transformation of spatially uniform input considered in Figs. 3(d), 3(e) was not reliable: While the first PC projection reliably tracked the input, other components were highly unreliable from trial to trial [Figs. 4(a), 4(b)]. We conjectured that this unreliability is due to the spatial symmetry of the network: Since the activity patterns generated by the unstable network arise through a symmetry-breaking dynamic, there are numerous firing rate patterns that are equally likely to be evoked each time the input is presented. As a result, the

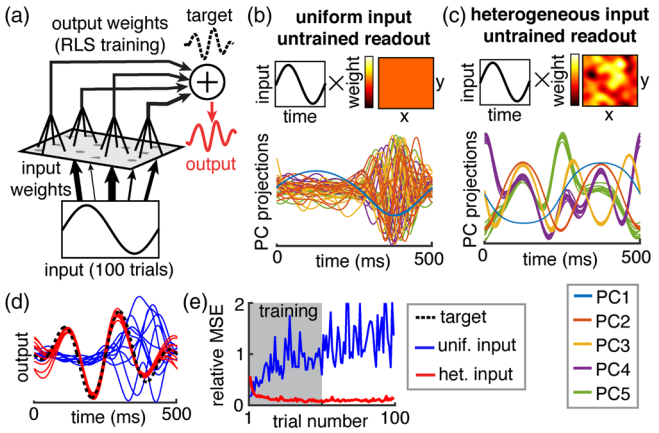


FIG. 4. Reliable computations require heterogeneous input. (a) Schematic. Same as Fig. 3(a) except the input was repeated for 100 consecutive trials and multiplied by fixed, location-dependent weights. Readouts were multiplied by output weights that were trained to produce a target output. (b) Overlaid plots of the first five PC projections of untrained readouts (uniform readout weights) over ten randomly selected trials when inputs were spatially uniform [same model as Fig. 3(d)]. (c) Same as (b) with spatially heterogeneous input weights. (d) Trained output from last ten trials with uniform (blue) and heterogeneous (red) input weights, compared to target (dashed black). (e) Mean-squared error of readouts.

evoked response depends on small differences in the network state when the input arrives.

We, therefore, considered an input that projects to the network with weights that vary across space [42] [Figs. 4(a), 4(c)]. This modification had a striking effect on the network response. Unlike the response to spatially uniform input, the response to spatially heterogeneous input was highly reliable from one presentation of the stimulus to another [Fig. 4(c)].

We next asked whether the unstable network could be trained to implement dynamical computations using the local rate readouts as the "reservoir" in a reservoir computing framework. Local rate readouts were linearly combined to produce an output time series. Readout weights were trained using a recursive least-squares algorithm [43] that iteratively updates weights to mold the output to a target time-series [44] [Fig. 4(a)].

When this algorithm was applied to firing rates produced by spatially uniform inputs [from Fig. 4(b)], the outputs did not produce the target time series [Figs. 4(d), 4(e), blue curves], due to the unreliability of the network response. When the same algorithm was applied to the rates produced by spatially heterogeneous inputs [from Fig. 4(c)], the outputs closely matched the target [Figs. 4(d), 4(e), red curves]. Further simulations show that the network can learn a variety of target outputs from a variety of inputs and that a slow adaptation current improves the networks' computational capabilities [45].

*Discussion.*—There is extensive literature on spatially extended neural fields [26–28] and the dynamics of spiking neuron models [46,47], but these topics are rarely combined. Previous studies found spatiotemporal dynamics in spiking networks with synaptic kinetics or delays [29,48,49]. Since the resonance for a Turing-Hopf bifurcation arises primarily from synaptic dynamics in these models, their stability is captured by differential neural field equations. The Turing-Hopf bifurcation observed here and in previous work [9] arises from the resonance of spiking neurons, which is not captured by differential neural field equations. Spatial dynamics arising from the resonance of neurons are rendered mathematically tractable by extending linear response techniques developed for homogeneous networks [34]. This approach is applicable to the growing class of neuron models for which the linear response function can be computed [22–24].

A few studies have implemented reservoir computing with spiking networks. Maass *et al.* [50] used a spatially extended spiking network for reservoir computing, but did not explain the role of spatial topology, which we have clarified. More recent studies [51,52] showed that precisely tuning a subnetwork of slow synapses offline can produce intricate rate dynamics in spiking networks. One of those studies [52], implemented reservoir computing with a spiking network. In the other study [51] this was only done for a rate network version of the model. It remains to be shown how this precise tuning of synapses could be achieved biologically, but inhibitory plasticity is one possibility [53].

Ostojic [54] showed that spiking networks can produce high-dimensional rate dynamics when synapses are strong, analogous to rate networks [55], but the reliability of these dynamics and their computational capabilities were not explored. The combination of strong coupling with spatial network topology is a promising direction for future study.

Distance-dependent connectivity is ubiquitous in the brain [13–16]. We showed that this spatial topology imparts spiking neural networks with the ability to perform dynamical computations (Fig. 4) while maintaining the ability to accurately track network input [Figs. 3(i), 3(j)]. Hence, spatial network architecture provides a critical link between biological realism and computational capability in recurrent neural network models.

Spatially extended networks are often modeled with integrodifferential equations that do not capture the history dependence of rate dynamics. We showed that this shortcoming is overcome using linear response theory to replace the integrodifferential equation (1) with an integral equation, (2). This approach has applications in any stochastic system with spatially and temporally nonlocal interactions such as models of social networks, population dynamics, and epidemiology.

We thank Ashok Litwin-Kumar, Bard Ermentrout, and Brent Doiron for helpful comments. This work was supported by NSF Grant No. DMS-1517828.

[1] W. R. Softky and C. Koch, J. Neurosci. **13**, 334 (1993).
[2] M. N. Shadlen and W. T. Newsome, Curr. Opin. Neurobiol. **4**, 569 (1994).
[3] C. van Vreeswijk and H. Sompolinsky, Science **274**, 1724 (1996).
[4] C. van Vreeswijk and H. Sompolinsky, Neural Comput. **10**, 1321 (1998).
[5] N. Brunel, J. Comput. Neurosci. **8**, 183 (2000).
[6] A. Renart, J. de La Rocha, P. Bartho, L. Hollender, N. Parga, A. Reyes, and K. Harris, Science **327**, 587 (2010).
[7] M. Monteforte and F. Wolf, Phys. Rev. X **2**, 041007 (2012).
[8] G. Lajoie, K. K. Lin, and E. Shea-Brown, Phys. Rev. E **87**, 052901 (2013).
[9] R. Rosenbaum and B. Doiron, Phys. Rev. X **4**, 021039 (2014).
[10] R. Pyle and R. Rosenbaum, Phys. Rev. E **93**, 040302 (2016).
[11] M. M. Churchland, J. P. Cunningham, M. T. Kaufman, J. D. Foster, P. Nuyujukian, S. I. Ryu, and K. V. Shenoy, Nature (London) **487**, 51 (2012).
[12] K. V. Shenoy, M. Sahani, and M. M. Churchland, Annu. Rev. Neurosci. **36**, 337 (2013).
[13] J. S. Lund, A. Angelucci, and P. C. Bressloff, Cereb. Cortex **13**, 15 (2003).
[14] R. B. Levy and A. D. Reyes, J. Neurosci. **32**, 5609 (2012).
[15] M. Ercsey-Ravasz, N. T. Markov, C. Lamy, D. C. VanEssen, K. Knoblauch, Z. Toroczkai, and H. Kennedy, Neuron **80**, 184 (2013).
[16] K. Knoblauch, M. Ercsey-Ravasz, H. Kennedy, and Z. Toroczkai, in *Micro-, Meso-and Macro-Connectomics of the Brain*, edited by H. Kennedy, D. C. Van Essen, and Y. Christen (Springer, Heidelberg, 2014), p. 45.
[17] M. R. Ricard and S. Mischler, J. Nonlinear Sci. **19**, 467 (2009).
[18] A. Roxin, N. Brunel, and D. Hansel, Phys. Rev. Lett. **94**, 238103 (2005).
[19] Membrane potential of neuron $j$ in population $a = e$, $i$ obeys $V' = -(V - E_L)/\tau_m + I_j^a$, where $E_L = -70$ mV, $\tau_m = 20$ ms, and each time $V$ exceeds $V_{th} = -50$ mV, a spike is recorded and $V$ is reset to $V_{re} = -75$ mV. In all simulations, average connection probabilities were $\bar{p}_{ee} = \bar{p}_{ie} = 0.0125$, $\bar{p}_{ei} = \bar{p}_{ii} = 0.05$, so that each neuron received 500 excitatory and 500 inhibitory inputs on average and connection weights were $j_{ee} = 0.1$, $j_{ie} = 0.2$, and $j_{ei} = j_{ii} = -0.25$ mV.
[20] $W = [w_{ee}(\mathbf{u})\ w_{ei}(\mathbf{u}); w_{ie}(\mathbf{u})\ w_{ii}(\mathbf{u})]$ is a $2 \times 2$ matrix function, where $w_{ab}(\mathbf{u}) = j_{ab} p_{ab}(\mathbf{u}) N_b$ and similarly for $U(\mathbf{u})$, except that $u_{ab} = j_{ab} w_{ab}$.
[21] D. Amit and N. Brunel, Cereb. Cortex **7**, 237 (1997).
[22] M. J. E. Richardson, Phys. Rev. E **76**, 021919 (2007).
[23] M. J. E. Richardson, Phys. Rev. E **80**, 021928 (2009).
[24] R. Rosenbaum, Front. Comput. Neurosci. **10**, 39 (2016).
[25] See Supplemental Material at http://link.aps.org/supplemental/10.1103/PhysRevLett.118.018103, Fig. 1 for a comparison with Poisson spike trains.
[26] B. Ermentrout, Rep. Prog. Phys. **61**, 353 (1998).
[27] S. Coombes, Biol. Cybern. **93**, 91 (2005).
[28] P. C. Bressloff, J. Phys. A **45**, 033001 (2012).
[29] S. Sadeh and S. Rotter, PLoS One **9**, e114237 (2014).
[30] S. Sadeh, C. Clopath, and S. Rotter, PLoS One **10**, e0127547 (2015).
[31] See Supplemental Material at http://link.aps.org/supplemental/10.1103/PhysRevLett.118.018103, Fig. 2.
[32] See Supplemental Material at http://link.aps.org/supplemental/10.1103/PhysRevLett.118.018103, Note S.1 and Fig. 4 for a review of the stability analysis of the neural field model.
[33] B. Lindner, Phys. Rep. **392**, 321 (2004).
[34] E. Ledoux and N. Brunel, Front. Comput. Neurosci. **5**, 25 (2011).
[35] See Supplemental Material at http://link.aps.org/supplemental/10.1103/PhysRevLett.118.018103, Note S.2 for a derivation.
[36] $A(\tau) = [A_e(\tau)0; 0A_i(\tau)]$, where $A_a(\tau)$ is the excitatory neurons' linear response to a perturbation in mean input, and similarly for $B(\tau)$.
[37] T. Kapitula and B. Sandstede, Discrete Contin. Dyn. Syst. **10**, 857 (2004).
[38] $\tilde{W} = [\tilde{w}_{ee}\ \tilde{w}_{ei}; \tilde{w}_{ie}\ \tilde{w}_{ii}]$ where $\tilde{w}_{ab}(\mathbf{n}) = j_{ab} N_b \bar{p}_{ab} \times \exp(-2\pi^2 \|\mathbf{n}\|^2 \sigma_b^2)$, similarly for $\tilde{U}$ and $\tilde{u}_{ab}(\mathbf{n}) = j_{ab} \tilde{w}_{ab}(\mathbf{n})$. Also, $\hat{A}(\lambda) = [\hat{A}_e(\lambda)\ 0; 0\ \hat{A}_i(\lambda)]$, where $\hat{A}_x(\lambda)$ is the susceptibility of excitatory neurons and similarly for $\hat{B}(\lambda)$.
[39] H. Risken, *The Fokker-Planck Equation* (Springer-Verlag, Berlin, 1989).
[40] See Supplemental Material at http://link.aps.org/supplemental/10.1103/PhysRevLett.118.018103, Fig. 3.
[41] See Supplemental Material at http://link.aps.org/supplemental/10.1103/PhysRevLett.118.018103, Fig. 1 for a comparison with Poisson spike trains.
[42] $F_j^e(t) = 3 + 1.5\sin(2\pi t) Q(x,y)$, where $Q(x,y)$ is a realization of quenched, spatial Gaussian noise with $E[Q(\mathbf{x})] = 0$, $E[Q(\mathbf{x})Q(\mathbf{x}+\mathbf{u})] = \exp[-|\mathbf{u}|^2/(2\sigma^2)]$, and $\sigma = 0.1$.
[43] D. Sussillo and L. F. Abbott, Neuron **63**, 544 (2009).
[44] See Supplemental Material at http://link.aps.org/supplemental/10.1103/PhysRevLett.118.018103, Note S.3 for description of numerical procedure for training weights.
[45] See Supplemental Material at http://link.aps.org/supplemental/10.1103/PhysRevLett.118.018103, Fig. 5 for further reservoir computing examples.
[46] W. Gerstner and W. M. Kistler, *Spiking Neuron Models: Single Neurons, Populations, Plasticity* (Cambridge University Press, Cambridge, England, 2002).
[47] E. M. Izhikevich, *Dynamical Systems in Neuroscience* (MIT Press, Cambridge, MA, 2007).
[48] S. Lim and M. S. Goldman, Nat. Neurosci. **16**, 1306 (2013).
[49] A. Keane and P. Gong, J. Neurosci. **35**, 1591 (2015).
[50] W. Maass, T. Natschläger, and H. Markram, Neural Comput. **14**, 2531 (2002).
[51] G. Hennequin, T. P. Vogels, and W. Gerstner, Neuron **82**, 1394 (2014).
[52] L. F. Abbott, B. Depasquale, and R.-m. Memmesheimer, Nat. Neurosci. **19**, 350 (2016).
[53] T. P. Vogels, H. Sprekeler, F. Zenke, C. Clopath, and W. Gerstner, Science **334**, 1569 (2011).
[54] S. Ostojic, Nat. Neurosci. **17**, 594 (2014).
[55] H. Sompolinsky, A. Crisanti, and H. J. Sommers, Phys. Rev. Lett. **61**, 259 (1988).

# Supplementary Materials for:
# Spatiotemporal dynamics and reliable computations in recurrent spiking neural networks

Ryan Pyle and Robert Rosenbaum

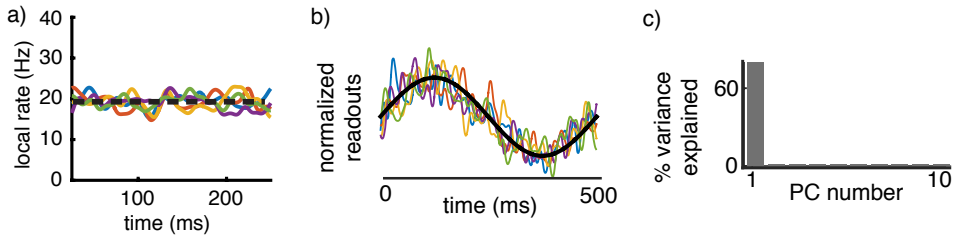


Supplementary Figure 1: **Comparison of stable network to population of Poisson-spiking neurons. a)** Same as Fig. 1b of main text, except all spike trains were replaced by homogeneous Poisson processes with firing rates equal to the population-wide average excitatory firing rate. Average temporal variance of readout = 3.4 $Hz^2$ in (a) and 3.6 $Hz^2$ in Fig. 1b. **b,c)** Same as Fig. 3b,c except all spike trains were replaced by inhomogeneous Poisson processes with firing rates equal to the time-dependent population-wide average excitatory firing rate.

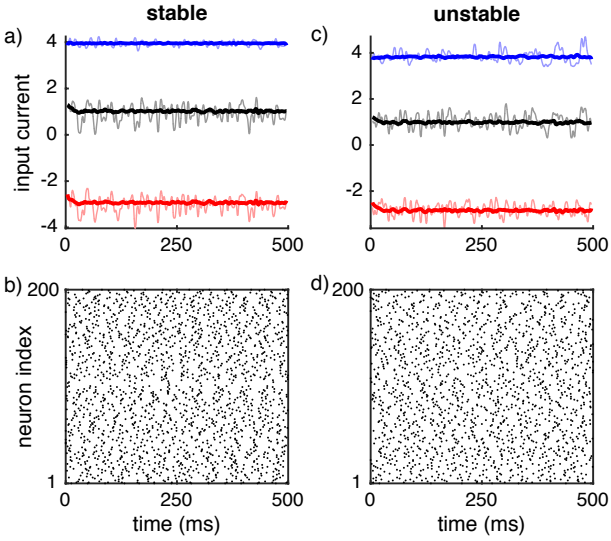


Supplementary Figure 2: **Input currents and spike train rasters from stable and unstable networks. a)** Excitatory (blue), inhibitory (red) and total (black/gray) input currents to excitatory neurons in the stable network from Fig. 1a–c. Thicker, dark curves are from averaging the input currents to 100 randomly selected excitatory neurons. Thinner, lighter curves are from a single randomly selected excitatory neuron. All currents were low-pass filtered (Gaussian kernel with width parameter $\sigma = 2$ms). **b)** Raster plot from 200 randomly selected excitatory neurons. **c,d)** Same as a and b, except for the unstable network from Fig. 1d-f.

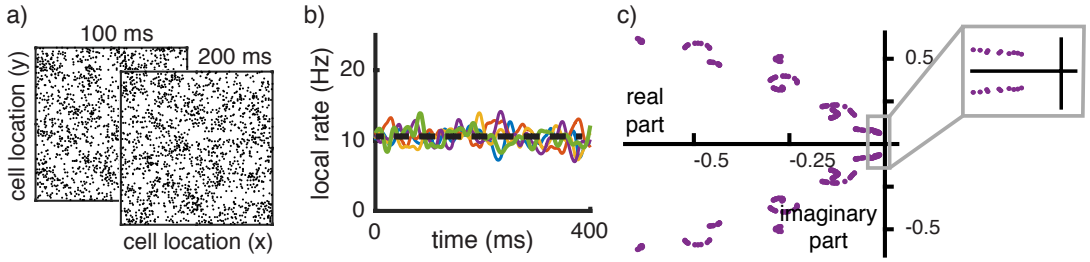


Supplementary Figure 3: **Stability achieved by increasing external input to inhibitory neurons. a,b,c)** Same as Fig. 1e, Fig. 1f and Fig. 2c of the main text respectively, except the external input to inhibitory neurons was increased by 25% ($F^{\mathrm{i}} = 2.875\mathrm{V/s}$), which caused the uniform fixed point to become stable.

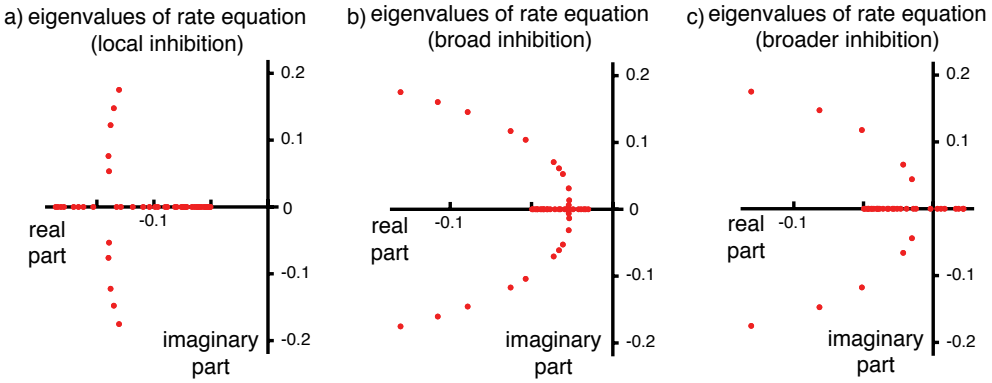


Supplementary Figure 4: **Eigenvalues of heuristic rate model. a)** Eigenvalues of rate model from Eq. (S.1) for the network with narrow inhibition from Figure 1a-c. **a)** Same as (a), but for the network with broad inhibition from Figure 1d-f. **c)** Same as (b), but with even broader inhibition, $\sigma_{\mathrm{i}} = 0.15$.

## S.1. STABILITY ANALYSIS OF THE INTEGRO-DIFFERENTIAL NEURAL FIELD MODEL

A heuristic stability analysis is given by considering the system of integro-differential equations [1–3]

$$\begin{aligned}\tau\frac{\partial\vec{r}(\mathbf{x},t)}{\partial t} &= -\vec{r}+\phi(\vec{\mu},\vec{v})\\ &= -\vec{r}+\phi\left(\iint_{\Gamma} W(\mathbf{u})\vec{r}(\mathbf{x}-\mathbf{u})d\mathbf{u}+\vec{F}(\mathbf{x}),\ \iint_{\Gamma} U(\mathbf{u})\vec{r}(\mathbf{x}-\mathbf{u})d\mathbf{u}\right)\end{aligned} \tag{S.1}$$

where $\tau > 0$ can be set to the membrane time constant of the neurons, $\tau = \tau_m$, but does not affect stability. The matrix integral kernels, $W$ and $U$, are given by [2]

$$W = \begin{bmatrix} w_{\mathrm{ee}}(\mathbf{u}) & w_{\mathrm{ei}}(\mathbf{u}) \\ w_{\mathrm{ie}}(\mathbf{u}) & w_{\mathrm{ii}}(\mathbf{u}) \end{bmatrix} \text{ and } U = \begin{bmatrix} u_{\mathrm{ee}}(\mathbf{u}) & u_{\mathrm{ei}}(\mathbf{u}) \\ u_{\mathrm{ie}}(\mathbf{u}) & u_{\mathrm{ii}}(\mathbf{u}) \end{bmatrix}$$

with $w_{ab}(\mathbf{u}) = j_{ab}p_{ab}(\mathbf{u})N_b$ and $u_{ab}(\mathbf{u}) = j_{ab}w_{ab}(\mathbf{u})$. This system of integro-differential equations has the same fixed point firing rates computed through the diffusion approximation, but we next show that it does not accurately predict stability of this fixed point.

The stability of a fixed point to Eq. (S.1) is given by transitioning to the Fourier domain and computing the Jacobian matrix

$$\widetilde{J}(\mathbf{n}) = \frac{1}{\tau}\left[-Id\,\delta_{\mathbf{n}} + G\widetilde{W}(\mathbf{n}) + H\widetilde{U}(\mathbf{n})\right]$$

at each spatial two-dimensional Fourier mode, $\mathbf{n} = (n_1, n_2)$ where $Id$ is the $2\times 2$ identity matrix and $\delta_{\mathbf{n}} = 1$ when $\mathbf{n} = (0,0)$ and 0 otherwise. Spatial synaptic filtering is captured by the matrices

$$\widetilde{W}(\mathbf{n}) = \begin{bmatrix} \widetilde{w}_{\mathrm{ee}}(\mathbf{n}) & \widetilde{w}_{\mathrm{ei}}(\mathbf{n}) \\ \widetilde{w}_{\mathrm{ie}}(\mathbf{n}) & \widetilde{w}_{\mathrm{ii}}(\mathbf{n}) \end{bmatrix} \text{ and } \widetilde{U}(\mathbf{n}) = \begin{bmatrix} \widetilde{u}_{\mathrm{ee}}(\mathbf{n}) & \widetilde{u}_{\mathrm{ei}}(\mathbf{n}) \\ \widetilde{u}_{\mathrm{ie}}(\mathbf{n}) & \widetilde{u}_{\mathrm{ii}}(\mathbf{n}) \end{bmatrix}.$$

Here, $\widetilde{w}_{ab}(\mathbf{n}) = j_{ab}N_b\overline{p}_{ab}\exp(-2\pi^2\|\mathbf{n}\|^2\sigma_b^2)$ is the two-dimensional spatial Fourier series of $w_{ab}(\mathbf{x})$ at Fourier mode, $\mathbf{n}$ and similarly for $\widetilde{u}_{ab}(\mathbf{n}) = j_{ab}^2N_b\overline{p}_{ab}\exp(-2\pi^2\|\mathbf{n}\|^2\sigma_b^2)$ [2]. The matrices $G$ and $H$ represent the sensitivity of $\phi(\mu, v)$ with respect to changes in $\mu$ and $v$,

$$G = \begin{bmatrix} g_e & 0 \\ 0 & g_i \end{bmatrix} \text{ and } H = \begin{bmatrix} h_e & 0 \\ 0 & h_i \end{bmatrix}$$

where

$$g_a = \left.\frac{\partial\phi}{\partial\mu}\right|_{\mu,v=\mu_a^0,v_a^0} \text{ and } h_a = \left.\frac{\partial\phi}{\partial v}\right|_{\mu,v=\mu_a^0,v_a^0}$$

where $\mu_a^0$ and $v_a^0$ are the fixed point input mean and variance for population $a = \mathrm{e}, \mathrm{i}$.

Applying this stability analysis to both of the networks in Figure 1 of the main text gives eigenvalues with negative real part (Supplementary Figure 4a,b). Increasing the width of inhibition further causes an instability, but the eigenvalues with positive real part are real (Supplementary Figure 4c), indicating a Turing bifurcation instead of a Turing-Hopf. This Turing bifurcation gives rise to static patterns as observed in previous work [2].

### S.2. DERIVATION OF STABILITY ANALYSIS USING LINEAR RESPONSE THEORY.

Consider a perturbation away from the uniform fixed point, $\vec{r}(\mathbf{x}, t) = r_0 + \delta\vec{r}(\mathbf{x}, t)$. Since synaptic integration is linear, this firing rate perturbation produces a resulting perturbation in the mean and variance of neurons' inputs according to

$$\delta\vec{\mu}(\mathbf{x}, t) = \iint_\Gamma W(\mathbf{x}-\mathbf{u})\delta\vec{r}(\mathbf{u}, t)d\mathbf{u}$$
$$\delta\vec{v}(\mathbf{x}, t) = \iint_\Gamma U(\mathbf{x}-\mathbf{u})\delta\vec{r}(\mathbf{u}, t)d\mathbf{u}$$

where $W(\mathbf{u})$ and $U(\mathbf{u})$ are the same $2\times 2$ matrix integral kernels introduced in the main text. The mapping from a perturbation of neurons' input mean and variance to a perturbation of their firing rates is given to linear order by

$$\delta\vec{r}(\mathbf{x}, t) = \int_0^\infty [A(\tau)\delta\vec{\mu}(\mathbf{x}, t-\tau) + B(\tau)\delta\vec{v}(\mathbf{x}, t-\tau)]d\tau$$

where

$$A(\tau) = \begin{bmatrix} A_\mathrm{e}(\tau) & 0 \\ 0 & A_\mathrm{i}(\tau) \end{bmatrix} \quad \text{and} \quad B(\tau) = \begin{bmatrix} B_\mathrm{e}(\tau) & 0 \\ 0 & B_\mathrm{i}(\tau) \end{bmatrix}$$

and $A_x(\tau)$ and $B_x(\tau)$ are the linear response to perturbations in the input mean and variance of excitatory and inhibitory neurons ($x = \mathrm{e}, \mathrm{i}$). Combining these equations gives Eq. (2) from the main text, from which Eq. (3) of the main text is derived through a Fourier and Laplace transform. The susceptibility functions were computed numerically using the threshold-integration scheme [4–6]. Eq. (3) of the main text is a transcendental equation in the complex plane, which we numerically solved at each wave number, $|\mathbf{n}|$, using Newton's method with a lattice of different initial values, $\lambda$.

### S.3. REVIEW OF RECURSIVE LEAST SQUARES PROCEDURE FOR TRAINING SYNAPTIC WEIGHTS

Learning in Fig. 4 of the main text was implemented using the same recursive least squares (RLS) scheme used in previous reservoir computing models [7], except there was no feedback from the output to the reservoir network in our model. The output was defined as

$$y(t) = \sum_k w_k x_k(t)$$

where

$$x_k(t) = \sum_{t_i\in G_k} \eta(t-t_i), \quad k = 1, \ldots, 100,$$

$$\eta(t) = \frac{1}{\sqrt{2\pi}\sigma} e^{-t^2/(2\sigma^2)},$$

$t_i$ are the spike times of neurons in group $k$ and $\sigma = 30$ ms. During learning, weights were updated at each time step according to

$$\Delta\vec{w} = -E\vec{x}P$$

where $E(t) = y(t) - f(t)$ is the error, $f(t)$ is the target and the matrix $P(t)$ is updated by

$$\Delta P = -\frac{\beta}{1 + \vec{x}P\vec{x}^T} P\vec{x}\vec{x}^T P$$

using time step of 1 ms and learning rate of $\beta = 1$. Learning was turned off halfway through each simulation by freezing $\vec{w}$ after the 50th trial.

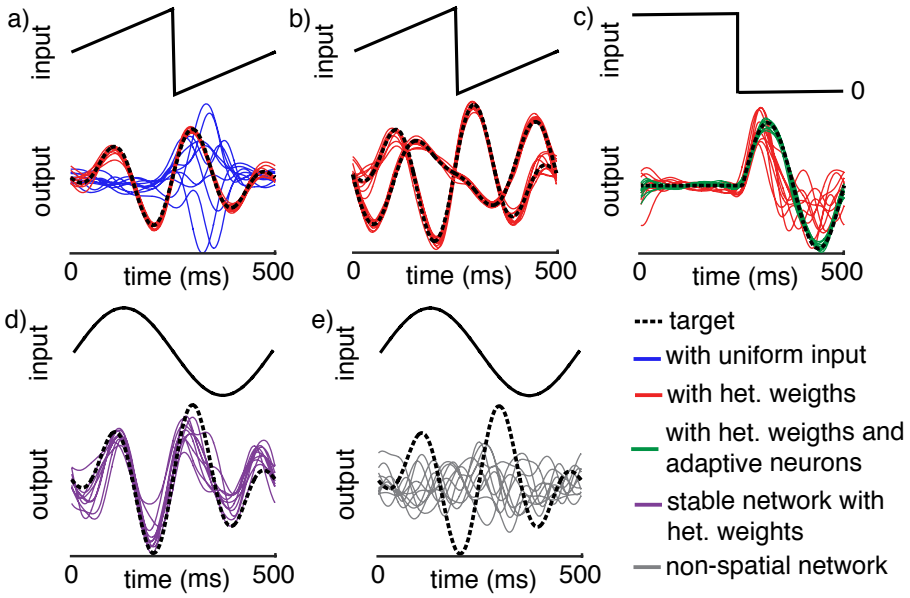


Supplementary Figure 5: **Additional reservoir computing examples. a)** Same as Fig. 5b of the main text, but sinusoidal input was replaced with a sawtooth (top) with the same amplitude. Accuracy improved when inputs were heterogeneous (average post-learning relative MSE = 0.021 in (a, red) and 0.11 in Fig. 5b red). **b)** Same as (a), but two sets of readout weights were trained simultaneously to produce two target outputs. **c)** Same as (a), but target was zero before 250 ms and input is zero after 250 ms. The network with heterogeneous input performed poorly (red), indicating a lack of short term memory in the spontaneous dynamics of the network. However, adding an adaptation current to the neuron models improved performance (green). Adaptation was added by changing membrane potential equation to $V' = -(V - E_L)/\tau_m + I - w$ where $\tau_w w' = -w$ and $w \to w + b$ at each spike with $\tau_w = 150$ ms and $b = 0.3$ V/s. **d)** Same as Fig. 5b red except using the network connectivity from Fig. 1a,b, in which inhibition projects more narrowly than excitation. Average post-learning relative MSE increased to 0.28 (from 0.11 in Fig. 5b red). We conjecture that the network with narrow inhibition was able to approximate the target because the spatially heterogeneous input de-stabilizes network dynamics by changing neurons' linear response functions in a spatially heterogeneous way. **e)** Same as (d) except for network with spatially unstructured recurrent connectivity and input. In particular, we used a network with random, spatially unstructured connections (with the same network-averaged connection probabilities as the spatial networks) and we used spatially uniform input weights. Average post-learning MSE was 1.2. We conclude that spatially coherent dynamics overcome the difficulty of reservoir computing with spiking networks.

[1] B. Ermentrout, Rep. Prog. Phys **61**, 353 (1998).
[2] R. Rosenbaum and B. Doiron, Phys Rev X **4**, 021039 (2014).
[3] S. Ostojic, Nat. Neurosci. **17**, 594 (2014).
[4] M. J. E. Richardson, Phys Rev E **76**, 021919 (2007).
[5] M. J. E. Richardson, Phy Rev E **80**, 021928 (2009).
[6] R. Rosenbaum, Front Comput Neurosci **10**, 39 (2016).
[7] D. Sussillo and L. F. Abbott, Neuron **63**, 544 (2009).